



Article

Electrochemical Synthesis and Application of Ge-Sn-O Nanostructures as Anodes of Lithium-Ion Batteries

Ilya M. Gavrilin ^{1,*}, Yulia O. Kudryashova ¹, Maksim M. Murtazin ², Ilia I. Tsiniakin ^{3,4}, Alexander V. Pavlikov ⁴ , Tatiana L. Kulova ¹ and Alexander M. Skundin ¹

¹ Frumkin Institute of Physical Chemistry and Electrochemistry, Leninsky Prospect, 119071 Moscow, Russia; yulia.kudryashova@mail.ru (Y.O.K.); tkulova@mail.ru (T.L.K.); askundin@mail.ru (A.M.S.)

² Institute of Advanced Materials and Technologies, National Research University of Electronic Technology—MIET, Shokin Square, 124498 Moscow, Russia; nizatruum@yandex.ru

³ MSU Quantum Technology Centre, 119991 Moscow, Russia; ii.tcinyaykin@physics.msu.ru

⁴ Physics Department, M.V. Lomonosov Moscow State University, 119991 Moscow, Russia; pavlikov@physics.msu.ru

* Correspondence: gavrilin.ilya@gmail.com

Abstract: This work demonstrates the possibility of electrochemical formation of Ge-Sn-O nanostructures from aqueous solutions containing germanium dioxide and tin (II) chloride at room temperature without prior deposition of fusible metal particles. This method does not require complex technological equipment, expensive and toxic germanium precursors, or binding additives. These advantages will make it possible to obtain such structures on an industrial scale (e.g., using roll-to-roll technology). The structural properties and composition of Ge-Sn-O nanostructures were studied by means of scanning electron microscopy and X-ray photoelectron spectroscopy. The samples obtained represent a filamentary structure with a diameter of about 10 nm. Electrochemical studies of Ge-Sn-O nanostructures were studied by cyclic voltammetry and galvanostatic cycling. Studies of the processes of lithium-ion insertion/extraction showed that the obtained structures have a practical discharge capacity at the first cycle ~625 mAh/g (specific capacity ca. 625 mAh/g). However, the discharge capacity by cycle 30 was no more than 40% of the initial capacity. The obtained results would benefit the further design of Ge-Sn-O nanostructures formed by simple electrochemical deposition.

Keywords: lithium-ion batteries; electrodeposition; germanium; tin



Citation: Gavrilin, I.M.;

Kudryashova, Y.O.; Murtazin, M.M.;

Tsiniakin, I.I.; Pavlikov, A.V.; Kulova,

T.L.; Skundin, A.M. Electrochemical

Synthesis and Application of

Ge-Sn-O Nanostructures as Anodes

of Lithium-Ion Batteries. *Appl. Nano*

2023, *4*, 178–190. [https://doi.org/](https://doi.org/10.3390/applnano4020010)

10.3390/applnano4020010

Academic Editor: Victor Burlakov

Received: 22 April 2023

Revised: 29 May 2023

Accepted: 1 June 2023

Published: 7 June 2023



Copyright: © 2023 by the authors.

Licensee MDPI, Basel, Switzerland.

This article is an open access article

distributed under the terms and

conditions of the Creative Commons

Attribution (CC BY) license ([https://](https://creativecommons.org/licenses/by/4.0/)

[creativecommons.org/licenses/by/](https://creativecommons.org/licenses/by/4.0/)

4.0/).

1. Introduction

The development of portable electronics in the last few decades has led to a growing market for energy storage. In addition, the demand for various electric vehicles (from scooters to buses) has increased significantly in recent times. Among existing energy storage systems, lithium-ion batteries (LIB) are the most common in modern portable consumer electronics and are used as an energy source in electric vehicles and as energy storage in power systems [1]. However, due to the ever-increasing demands on energy density and lifetime, modern, scalable, cost-effective materials with high theoretical capacity and stable structure during multiple discharge/recharge cycles need to be developed [2].

Elements such as silicon (Si), tin (Sn), and germanium (Ge) are very promising materials for high-efficiency lithium-ion battery anodes because of their high theoretical capacity [3–7]. Although Ge is inferior to silicon in theoretical gravimetric specific capacitance (1624 mAh/g vs. 3579 mAh/g), their volumetric specific capacities are quite similar (7366 and 8334 mAh/cm³). At the same time, Ge has higher electronic conductivity than Si. Furthermore, the diffusion coefficient of Li⁺ ions in Ge is 400 times higher than in Si [8,9]. However, as with other high-capacity materials, the main disadvantage of germanium is its huge (over 350%) volumetric expansion during lithium insertion/extraction. This

phenomenon leads to cracking and pulverization with loss of electrical contact. Furthermore, repeated volume expansion and shrinkage lead to the destruction and repair of solid electrolyte interface (SEI) films, with electrolyte consumption and loss of capacity. One approach to overcome these troubles is to use nanomaterials [10]. In particular, Ge nanowires are used to prevent multiple crystal cell volume expansion when Li is introduced [11]. However, despite the high electrochemical characteristics of Ge nanowires, the possible production methods (chemical vapor deposition, thermal evaporation, vapor deposition with a critical liquid source, molecular beam epitaxy) are highly energy-consuming, technologically complicated, and also usually involve toxic and flammable gases (monogerman and hydrogen) [11–13]. Furthermore, the methods are high-temperature, which limits the range of substrates used for anodes. A promising solution to this problem is the use of electrochemical production methods. However, intensive hydrolysis of liquid precursors (e.g., GeCl_4) commonly used for electrochemical Ge deposition requires the use of non-aqueous solvents (e.g., ionic liquids or propylene glycol) of high purity and in an inert atmosphere [14,15]. In addition, the formation of arrays of Ge nanostructures from non-aqueous electrolytes requires the use of polycarbonate membranes [16] or self-ordered porous matrices such as aluminum oxide [17], which require additional technological operations to obtain and remove them. It is worth noting that the possibility of electrochemical deposition of 1D nanostructures without a template has been demonstrated in the literature. In particular, 1D nanostructures of tin (Sn), zinc (Zn), and tellurium (Te) have been obtained. An important role in the formation of such structures is played by special organic additives that stimulate crystal growth in one direction [18].

On the one hand, cathodic polarization of solid-state electrodes in aqueous solutions of germanium dioxide allows the formation of films only a few monolayers thick due to the high efficiency of the parallel reaction of hydrogen evolution [19]. On the other hand, the possibility of electrochemical deposition of Ge nanowires from aqueous GeO_2 solutions at room temperature has been demonstrated [20–22]. In particular, these electrodes demonstrate excellent features, namely room-temperature specific capacity of ca. 1300 mAh/g at 1C and 4C rates and about 850 mAh/g at 24C, as well as good low-temperature performance of 255 mAh/g at $-50\text{ }^\circ\text{C}$ [20]. This method does not require complex technological equipment and high temperatures, as well as expensive and toxic Ge precursors. GeO_2 is an intermediate product in the production of Ge, and its cost is significantly lower than that of crystalline Ge or its liquid and gaseous precursors. Furthermore, this method enables the formation of structures directly on the conducting substrate (current collectors for LIB), which eliminates the binder and related additional technological operations. A special feature of this method is the preliminary formation of fusible metal particles as nucleation sites on the electrode surface. Such particles serve as electrodes for the reduction of Ge ions to Ge^0 and their subsequent dissolution to form an eutectic melt. The continuous cathode reduction reaction provides concentration supersaturation of the melt, resulting in Ge crystallization at the border with the substrate [23]. Thus, at the liquid metal-substrate interface, Ge grows by analogy with the growth of whiskers in the gas phase by the well-known vapor-liquid-crystal mechanism [24]. In the literature, this mechanism has been called electrochemical liquid-liquid-solid semiconductor crystal growth.

On the one hand, the use of aqueous solutions implies the use of metals or alloys with a melting point of less than $100\text{ }^\circ\text{C}$, e.g., mercury (Hg), gallium (Ga), gallium-indium (GaIn), and bismuth-indium (BiIn) alloys [25–28]. On the other hand, the melting point can decrease as the size of the metal particles decreases [29]. In addition, the particle may not be completely molten but may have a core-shell structure, where the core is a solid phase and the shell is a liquid phase. Thus, fusible In particles can be successfully used as Ge nucleation sites (although the melting point of bulk In is approximately $156.6\text{ }^\circ\text{C}$) [20–22,30]. Another low-melting metal is tin (Sn), which has a slightly higher melting point ($\sim 232\text{ }^\circ\text{C}$) while being a cheaper and more common metal. However, the ability to form Ge nanowires using Sn particles at room temperature has not been demonstrated in the literature.

In this work, we have shown the possibility of the formation of tin-containing Ge nanowires at room temperature with a small current density of -2 mA/cm^2 and investigated their electrochemical properties as an anode in a lithium-ion battery.

2. Materials and Methods

2.1. Sample Preparation

A 40-micrometer-thick copper foil was used as the substrate and current collector. The foil was cut into $2 \times 3 \text{ cm}$ pieces. The foil was treated in acetone in an ultrasonic bath for 5 min, washed with deionized water, and dried in an argon flow. The reverse side of the foil was coated with a chemically resistant lacquer. Following that, the samples were air-dried for 30 min. Electrochemical deposition of Ge-Sn-O nanostructures was performed in a three-electrode cell. A platinum ring was used as a counter electrode, and a standard silver chloride electrode (Mettler-Toledo InLab Reference Flow) was used as the reference one. Electrochemical deposition of Ge-Sn-O nanostructures was performed in an aqueous electrolyte. The electrolyte for deposition was prepared by mixing 1 part of solution A and 4 parts of solution B. Solution A contained 0.02 M tin (II) chloride dihydrate ($\text{SnCl}_2 \cdot 2\text{H}_2\text{O}$, ACS reagent, 98%, Sigma-Aldrich, Saint Louis, MO, USA) and 0.3 M citric acid ($\text{C}_6\text{H}_8\text{O}_7$, ACS reagent, $\geq 99.5\%$, Sima-Aldrich, Saint Louis, MO, USA). The order in which the ingredients are mixed is important for the preparation of solution A. First, the ammonium hydroxide (NH_4OH , ACS reagent, 28.0–30.0% NH_3 basis) and deionized water were mixed in a 1:9 ratio. Following that, $\text{SnCl}_2 \cdot 2\text{H}_2\text{O}$ was added and stirred until completely dissolved. The citric acid was then added. After that, the solution was stirred for 15 min with a magnetic stirrer.

Solution B contained 0.05 M germanium dioxide (GeO_2 , 99, 998%, Germanium and Applications Ltd., Moscow, Russian), 0.5 M succinic acid ($\text{C}_4\text{H}_6\text{O}_4$, ACS reagent, $\geq 99.0\%$, Sigma-Aldrich, Saint Louis, MO, USA), and 0.05 M ammonium sulfate (NH_4SO_4 , ACS reagent, $\geq 99.0\%$, Sigma-Aldrich, Saint Louis, MO, USA). The solution B's pH was brought to 6.5 by adding NH_4OH . A further increase in the pH of the electrolyte solution leads to precipitation in the solution volume.

Deposition was performed at a solution temperature of $20 \text{ }^\circ\text{C}$ (maintained by a VT-01 thermostat, Termex, Tomsk, Russian) and a current density of -2 mA/cm^2 with the use of a potentiostat/galvanostat Autolab PGSTAT302N (Metrohm, Barendrecht, The Netherlands). The current was set taking into account the visible surface area of the sample. The obtained samples were washed in deionized water and dried in an argon flow. The precise weight of deposited Ge-Sn-O nanostructures was determined by the gravimetric method using the analytical balance Mettler Toledo XP 205 ($d = 0.01 \text{ mg}$, Mettler-Toledo International Inc., Greifensee, Switzerland).

Figure 1 shows a schematic representation of the formation of Ge-Sn-O nanostructures.

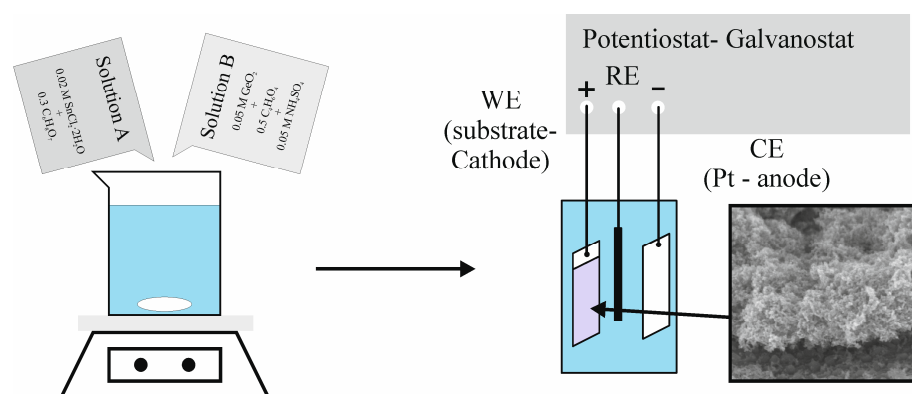


Figure 1. Schematic representation of the formation of Ge-Sn-O nanostructures.

2.2. Electrochemical Characterization

Electrochemical cells contained three electrodes: the working electrode (Ge-Sn-O nanostructure on a copper foil substrate), the counter electrode (lithium), and the reference (lithium). As a substrate for the counter electrode and the reference electrode, we used a nickel mesh with a nickel foil current lead welded to it. Working electrodes were pre-dried under vacuum at 120 °C for 8 h in a vacuum drying oven (DZF-6050, Shandong Gelon Lib Co., Ltd., Shandong, China). The apparent surface area of the electrodes was 1 cm². The Ge-Sn-O nanostructure loading was 100 µg/cm². The electrolyte used was 1M LiClO₄ in a propylene carbonate-dimethoxyethane mixture (7:3). The electrolytes were prepared from commercial salts and solvents (Aldrich-Sigma, battery grade, Saint Louis, MO, USA). The water content of the electrolyte measured by Fischer coulometric titration (917 Coulometer, Metrohm, Herisau, Switzerland) was not more than 15 ppm. The electrochemical cells were assembled in a sealed glove box (Spektroskopicheskie Sistemy, Moscow, Russia) with an argon atmosphere. The water and oxygen content in the box were about 1 ppm. Electrochemical studies of electrodes were carried out using the multichannel potentiostat P20-X8 (Elins, Chernogolovka, Russia).

2.3. Material Characterization

The structural properties were studied by a scanning electron microscope (SEM) of the Carl Zeiss SUPRA 40 FE-SEM (an Inlens SE detector was used, accelerating voltage = 10 kV, aperture = 30 µm, Oberkochen, Germany).

The elemental composition and chemical state of the detected elements were investigated by X-ray photoelectron spectroscopy (XPS) using a PHI5500 Versa Probe II spectrometer (with a monochromatized Al K α X-ray as the excitation source ($h\nu = 1486, 6$ eV), Physical Electronics, Inc. (PHI), Chanhassen, MN, USA). Argon ion sputtering of the surface samples was performed using 2 keV Ar⁺ ions with a raster size of 3 × 3 mm². The analysis area was 200 µm in diameter. The binding energies (E_b) of photoelectronic lines (C 1s, O 1s, Ge 3d, Ge 2p₃, and Sn 3d) were determined from high-resolution spectra taken at the transmittance energy of 23.5 eV. The calibration of the bonding energy scale was performed for Au 4f-83.96 eV and Cu 2p₃-932.62 eV. For the sample on the initial surface, the position of the Ge 3d peak from Ge⁰ is 29.6 eV (the reference value for pure germanium is 29.4 eV), so all spectra were shifted by minus 0.2 eV. After etching, the E_b scale was not corrected because the positions of peaks from metallic Ge and Sn matched the reference values. XPS data were analyzed with PHI MultiPak software. Concentrations were determined by the relative elemental sensitivity factor method using measured integral intensities of the following lines: C 1s, O 1s, Ge 3d, In 3d, K 2p, and Ti 2p.

3. Results

First of all, the samples were investigated by linear sweep voltammetry. Figure 2 shows the I-U curves of the obtained samples. The potential scan rate was 5 mV/s.

As can be seen, in the case of sample 1, there is practically no reaction up to a potential of −1.4 V, after which there is a sharp change in current density. This change corresponds to the evolution of hydrogen gas, which can be observed visually. In the case of sample 2, however, the picture is different. A clear cathodic peak is observed at −0.7 V. This peak is indicative of the reduction of Sn ions to Sn⁰. A further shift of the potential to more negative values results in a significant increase in the cathode current, which indicates the additional Ge ion reduction reaction. In this time period, a black film is visually observed on the electrode surface. Further deposition was carried out at a constant current density of −2 mA/cm², selected on the basis of I-U curves. Figure 3 shows the U-t curve for the deposition of Ge-Sn-O nanostructures on Cu foil.

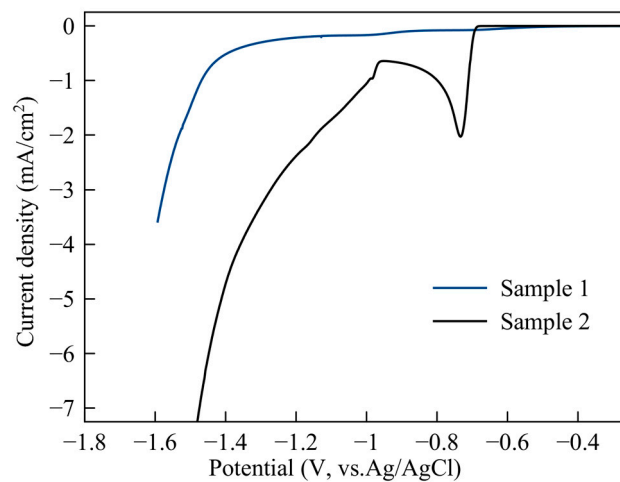


Figure 2. I-U curves of samples obtained in different electrolytes: sample 1 without $\text{SnCl}_2 \cdot 2\text{H}_2\text{O}$ and sample 2 with 0.02 M $\text{SnCl}_2 \cdot 2\text{H}_2\text{O}$. The potential scan rate was 5 mV/s.

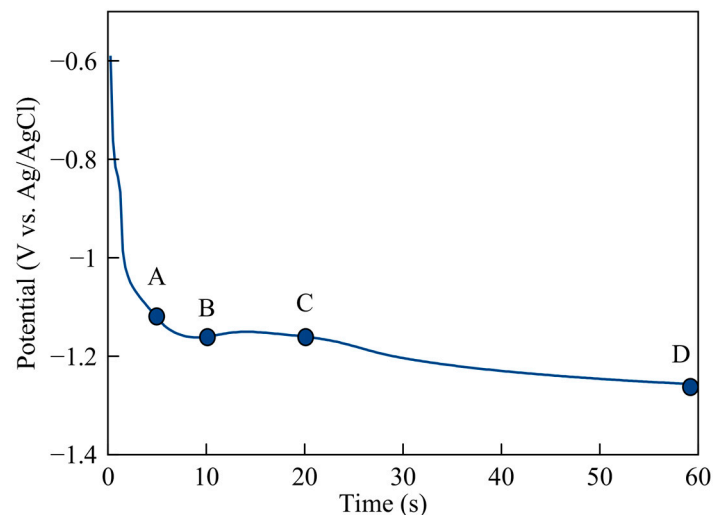


Figure 3. U-t curve for the deposition of Ge-Sn-O nanostructures at -2 mA/cm^2 .

The resulting curve shows characteristic areas of change in electrode potential over time. A small band is observed at a potential of -1.15 V , after which the potential changes into a more negative area until the end of the deposition process. This change in potential could indicate a change in the surface morphology of the sample. To verify this statement, samples with different deposition times were prepared according to selected points on the curve (Figure 3) and investigated by scanning electron microscopy. Figure 4 shows SEM images of the surface morphology of the samples after different deposition times.

Comparing the data in Figures 3 and 4, one can conclude that point A in the curve (Figure 3) corresponds to the deposition of Sn particles (Figure 4a(1)). As one can see, the particles are not spherical and reach sizes of about 100 nm in one direction. Furthermore, in some areas, particles as small as 10 nm can be observed (Figure 4a(2)). After the particle deposition, a filamentous structure with a diameter of about 10 nm is formed (Figure 4b(3)), which is much smaller than the Sn particle formed in the first step. Further increasing the process time leads to complete overgrowth of the surface by these structures (Figure 4c,d) and an increase in their thickness. It is also worth noting that the particles that were formed at the first stage do not participate in the layer formation process later on, as can be clearly seen in Figure 5.

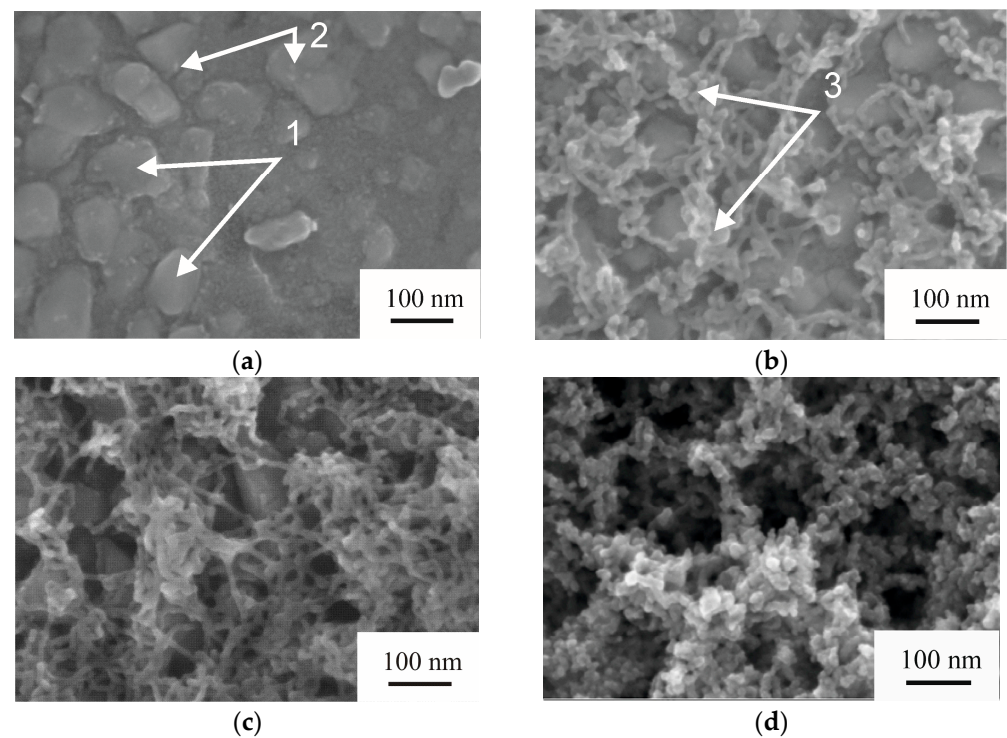


Figure 4. SEM images of the obtained Ge-Sn-O nanostructures at different process durations corresponded to the points at the U-t curve: (a) A, (b) B, (c) C, and (d) D. 1—Sn particles; 2—small particles; 3—filamentous nanostructure.

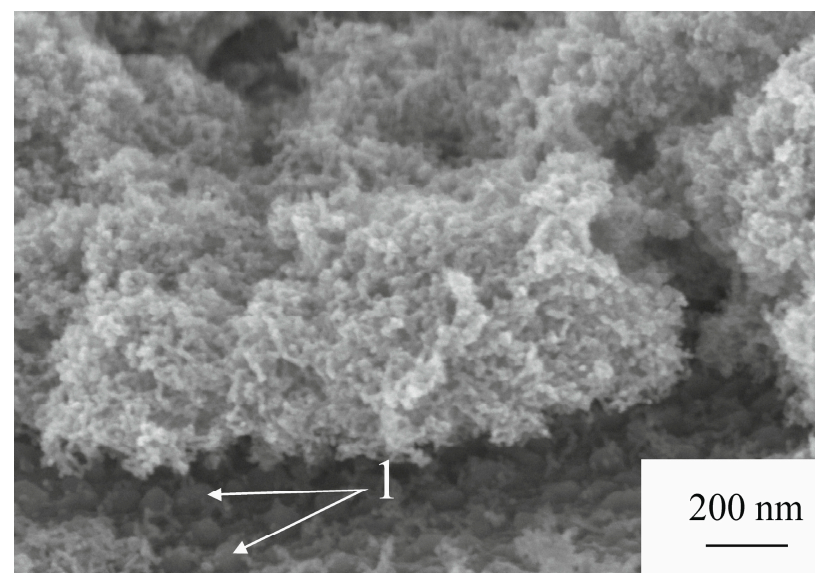


Figure 5. SEM images of the cross-section of the sample corresponded to the point D at the U-t curve. 1—Sn particles.

The surface composition of the Ge-Sn-O nanostructure was investigated with XPS. Figure 6 shows the survey XPS spectra of the sample that corresponded to the point D at the U-t curve before and after Ar ion sputtering.

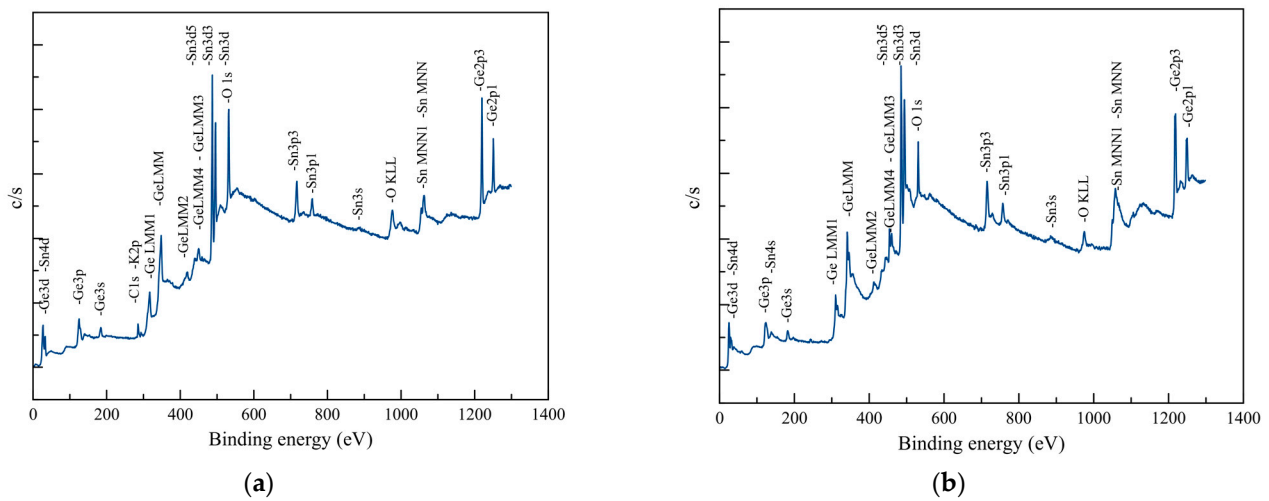


Figure 6. The survey spectrum of the Ge-Sn-O nanostructure before (a) and after (b) Ar ion sputtering of the surface.

The atomic concentrations before and after Ar ion sputtering of the surface sample are presented in Table 1.

Table 1. Surface atomic element concentrations from XPS analyses (at %).

| Etching Time, min | C | O | Ge | Sn | K |
|-------------------|----|----|----|----|---|
| - | 16 | 52 | 20 | 11 | 1 |
| 2 | - | 38 | 40 | 22 | - |

As can be seen, a large concentration of carbon (C), germanium (Ge), tin (Sn), and oxygen (O), as well as a small amount of potassium (K), is present on the surface of the sample. All these elements are part of the deposition bath solution. However, after Ar ion sputtering of the surface samples, the concentrations of C and K decreased to the sensitivity level of the detector. This suggests that C and K were surface contaminants. For a detailed analysis of the chemical state of the detected elements, namely Ge and Sn, high-resolution spectra of Ge 2p₃ and Sn 3d before and after etching were analyzed. The obtained spectra are shown in Figure 7.

The results of the analysis of the obtained high-resolution spectra are presented in Table 2.

Table 2. Parameters of the Ge 2p₃ and Sn 3d spectra ($E_b \pm 0.2$ eV).

| Etching Time | Spectrum Parameters | Ge 2p ₃ | | | Sn 3d | |
|--------------|---------------------|--------------------|--------|--------------------|-------------------|--------------------|
| | | 1 Ge ⁰ | 2 GeO | 3 GeO ₂ | 1 Sn ⁰ | 2 SnO ₂ |
| - | E_b , eV | 1217.3 | 1218.8 | 1220.3 | 485.0 | 487.0 |
| | % | 5 | 13 | 82 | 15 | 85 |
| 2 | E_b , eV | 1217.3 | 1219.5 | - | 485.0 | 486.8 |
| | % | 50 | 50 | - | 60 | 40 |

On the basis of the obtained data, it can be concluded that on the initial surface, 85% of Sn is oxidized, and after etching, the amount of oxide component decreased to 40% (E_b (Sn⁰) coincides with the reference value of 485.0 eV) [31]. Ge on the surface is also almost completely oxidized, and the largest amount (82%) is accounted for by GeO₂. Only a part (13%) of it falls on GeO. However, after etching, the amount of GeO oxide increased to 50%, and GeO₂ was absent within the sensitivity limits of the spectrometer detector (E_b (Ge⁰) coincides with the reference value of 1217.3 eV) [31,32].

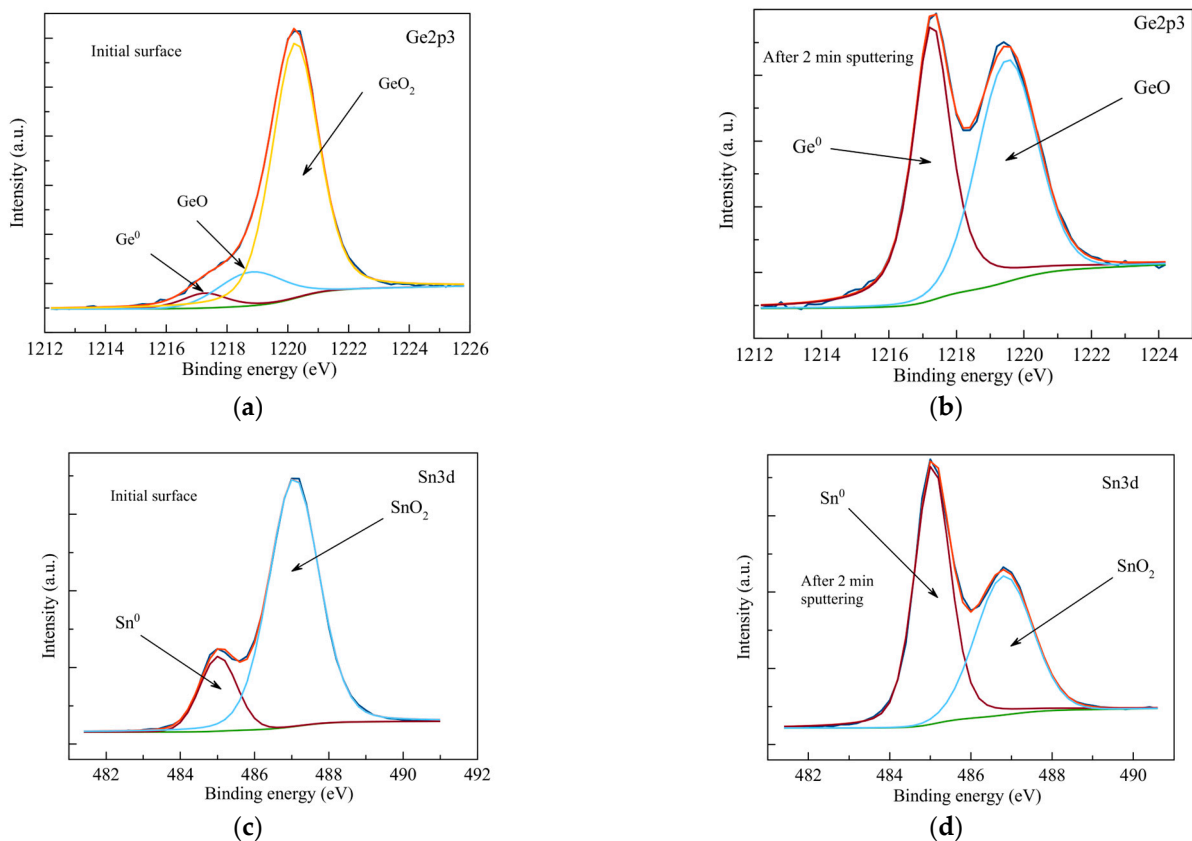
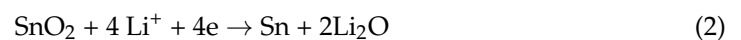
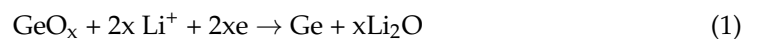


Figure 7. Deconvoluted Ge 2p3 (a,b) and Sn 3d5 (c,d) XPS high-resolution spectra before and after 2 min sputtering of the surface sample.

Electrochemical Studies of a Sample

All electrochemical measurements were carried out with a Ge-Sn-O sample that corresponded to point D on the U-t curve. Cyclic voltammetry is one of the most basic and versatile electrochemical tools that is widely used to identify the redox couples, describe the electrochemical processes, and investigate the reaction kinetics. Figure 8 shows cyclic voltammograms of Ge-Sn-O nanostructures for the first three cycles. In the first cycle, a large irreversible peak in the area of 1 V potential is registered at the cathode branches of cyclic voltammograms, which is associated with two processes: electrolyte reduction with the formation of a solid-electrolyte interface on the electrode surface [33,34] and reduction of partially oxidized Ge and Sn with the formation of Ge, Sn, and Li_2O [20,35,36]. These processes can be approximately expressed by the equations:



The current peaks in the cathodic cyclic voltammogram region at potentials around 0.59 and 0.19 V and the corresponding anodic peaks at potentials around 0.52 and 0.79 V are reversible and indicate the insertion/extraction processes of lithium into germanium and tin.

These processes can be approximately expressed by the equations:



The reversible capacity on the first cycle, calculated from the area under the anode part of the cyclic voltammograms, was 519 mAh/g.

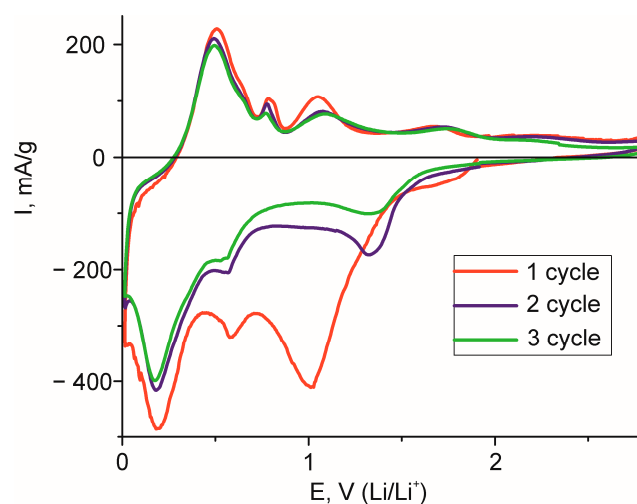


Figure 8. Cyclic voltammograms of the sample at a scan rate of 0.05 mV/s. The cycle numbers are shown in the figure.

Next, the samples were examined using galvanostatic cycling. The charge-discharge curves shown in Figure 9. During the first cathodic polarization, the shape of the curve differs significantly from the cathodic curves during subsequent cycles, which, as noted above, is related to the formation of a solid-electrolyte interface on the electrode surface and to the reduction of partially oxidized Ge and Sn. The shape of the anode curves undergoes some changes during cycling, which is associated with a decrease in the discharge capacity during cycling; in particular, the clear areas reflecting the process of Li extraction from Ge-Sn-O nanostructure disappear in the curves, and the average Li extraction potential also increases.

The dependence of the discharge (anode) capacity of the Ge-Sn-O nanostructure on the cycle number shows that the electrode degrades strongly at the initial cycles. Starting in cycle 10, the degradation rate decreases, and after cycle 30, the degradation becomes almost zero. The discharge capacity by cycle 30 is no more than 40% of the capacity at the first cycle, which was 625 mAh/g. Such a sharp drop in the discharge capacity is generally typical of Ge-based electrodes and is usually associated with the formation of an unstable solid-electrolyte interface. Such degradation can be further reduced by using an electrolyte containing a special organic additive [11,37]. The authors of [38] have reported some results of lithium insertion into Sn-modified nanoporous Ge. The initial reversible capacity for the composite Ge:Sn (3:1 atomic ratio) amounted to 1000 mAh/g; however, during the subsequent cycling with 200 mA/g, the reversible capacity dropped to 700 mAh/g. Figure 9b shows the variation of Coulombic efficiency (η) upon cycling. It is seen that the cathodic charge notably exceeds the anodic one not only at the first cycle but further up to the 30th cycle. This fact evidences permanent charge consumption for SEI formation and confirms the statement on SEI instability.

Figure 9c,d shows the electrochemical behavior of the Ge-Sn-O sample with a loading of 0.8 mg/cm². One can see that the samples with higher loading demonstrate lower initial discharge capacity (about 400 mAh/g even at the first cycle) and faster capacity fading. The Coulombic efficiency in this case remains less than 0.9 for the whole test (Figure 9d), which also testifies to SEI instability.

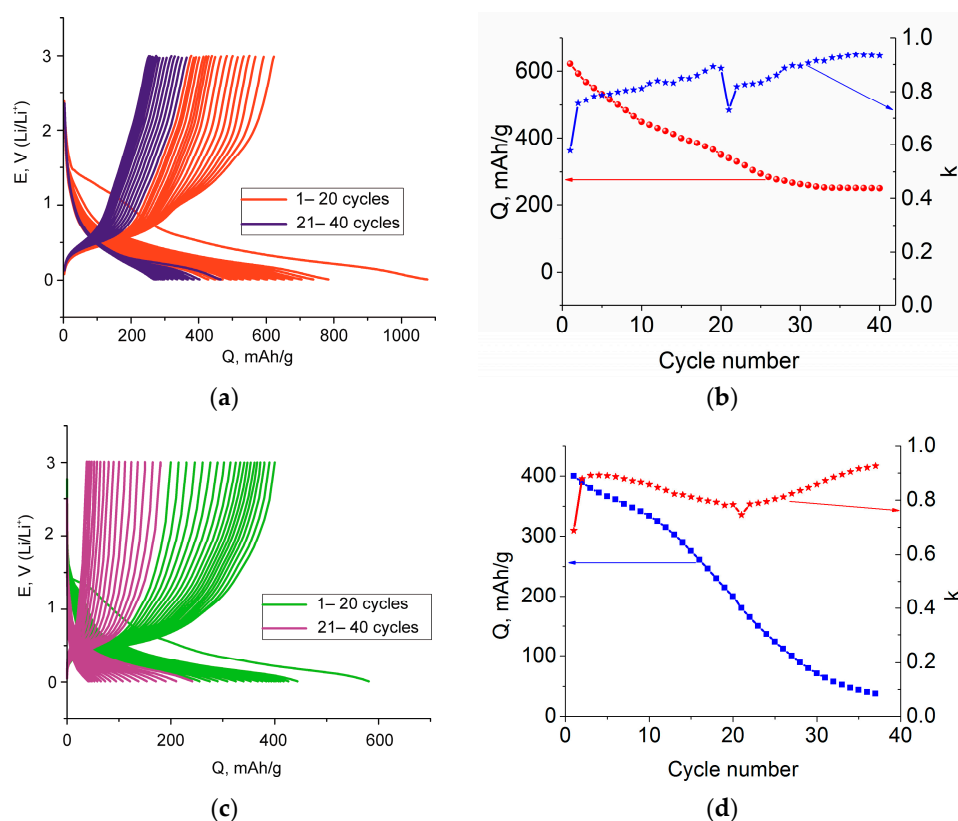


Figure 9. Charge and discharge profiles (a,c) and change discharge (anode) capacity during cycling (b,d, Red line—Coulombic efficiency; blue line—capacity) of the sample with loadings of 0.1 mg/cm² (a,b) and 0.8 mg/cm² (c,d). Current density of 250 mA/g. The number of cycles is shown in the figure.

4. Discussion

Based on the results, it was found that the addition of tin ions to the germanium deposition electrolyte promotes the formation of filamentous nanostructures on the copper substrate at room temperature. Analysis of the X-ray photoelectron spectroscopy results showed that the obtained sample is a mixture of partially oxidized Ge and Sn. The presence of oxides in the sample appears to be related to an increase in pH at the electrode-electrolyte interface due to a competing hydrogen reduction reaction, which has also been observed in the formation of Ge nanowires using In particles [20]. The mechanism of Ge-Sn-O nanostructure formation is not directly related to electrochemical liquid-liquid-solid crystal growth. Since the particles that are formed at the beginning of the process do not participate in the subsequent formation of the filamentous nanostructure (1-Figures 4a and 5). The authors in [39] showed that using Sn nanoparticles with a predominant size of ~10 nm and a process temperature of 90 °C, filamentous Ge nanostructures with a diameter of ~10 nm could be obtained. When the average size of tin nanoparticles was increased to 40 nm, nanowire crystals with diameters smaller than 10 nm were formed at some locations on the surface of Sn nanoparticles. In [40], it was stated that nanowire growth by the electrochemical liquid-liquid-solid mechanism is possible when using a mixed electrolyte solution (containing both Ge and Sn ions) without preliminary deposition of metal particles, but at rather high current densities of about 100–300 mA/cm². It is noted that such high current densities provide additional heating of the electrolyte at the electrode-electrolyte interface. Apparently, in this case, with such sizes of the particles and electrolyte temperature, there is no liquid phase that provides electrochemical liquid-liquid-solid growth of the filament, as is observed in the case of In or other fusible metals [21]. In turn, in a number of works, the possibility of co-deposition of Ge with metals (silver (Ag), copper (Cu), nickel (Ni), and cobalt (Co)) from aqueous solutions has been shown [41,42]. In [42], the authors suggest that induced co-deposition occurs through activation of the Ge-H

bond by Cu, possibly leading to the formation of adsorbed particles containing H-Cu-Ge, resulting in H dissociation, which leads to alloy growth in parallel with the formation of significant amounts of H₂ gas. It is possible that similar processes take place during the formation of Ge-Sn-O nanostructures. However, to find out the exact mechanism, more detailed studies are needed, which will be carried out in the future.

5. Conclusions

Thus, this work demonstrates the possibility of electrochemical formation of Ge-Sn-O nanostructures from aqueous solutions at room temperature without prior deposition of fusible metal particles. This method does not require complex technological equipment and high temperatures, as well as expensive and toxic Ge precursors. Furthermore, this method enables the formation of structures directly on the conducting substrate, which eliminates bonding agents and related additional technological operations. These advantages will make it possible to obtain such structures on an industrial scale (e.g., using roll-to-roll technology).

Studies of the processes of Li introduction and extraction showed that the obtained structures have a practical discharge capacity on the first cycle ~625 mAh/g. However, the discharge capacity by the 30th cycle was no more than 40% of the original capacity. Such degradation can be further reduced by using an electrolyte containing a vinylene carbonate additive. Furthermore, such anodes will be tested in sodium-ion batteries, which are currently the most promising.

In addition, future research will focus on the formation mechanism of Ge-Sn-O nanostructures and the possibility of controlling their geometrical parameters. In particular, detailed structural studies will make it possible to understand the nature of the various electrochemical processes involved in the formation of Ge-Sn-O nanostructures and to reveal the role of technological factors that influence these processes.

Author Contributions: I.M.G.—methodology, investigation, writing of original draft; Y.O.K.—investigation, visualization; M.M.M.—investigation; I.I.T.—investigation; A.V.P.—investigation, writing of original draft; T.L.K.—conceptualization, writing of original draft; A.M.S.—conceptualization, supervision. All authors have read and agreed to the published version of the manuscript.

Funding: The work was supported by a grant from the Russian Science Foundation No. 20-79-10312, <https://rscf.ru/en/project/20-79-10312/> (accessed on 20 July 2020).

Data Availability Statement: Not applicable.

Acknowledgments: The work was supported by the Interdisciplinary Scientific and Educational School of Moscow State University, “Photonic and Quantum Technologies. Digital Medicine”. The authors acknowledge the use of the research infrastructure of the “Educational and Methodical Center of Lithography and Microscopy” of M.V. Lomonosov Moscow State University. XPS measurements were carried out in the Collective Use Center “Materials Science and Metallurgy” of NUST MISiS.

Conflicts of Interest: The authors declare no conflict of interest.

References

1. Kim, T.; Song, W.; Son, D.-Y.; Ono, L.K.; Qi, Y. Lithium-ion batteries: Outlook on present, future, and hybridized technologies. *J. Mater. Chem. A* **2019**, *7*, 2942–2964. [[CrossRef](#)]
2. Mahmud, S.; Rahman, M.; Kamruzzaman, M.; Ali, M.O.; Emon, M.S.A.; Khatun, H.; Ali, M.R. Recent advances in lithium-ion battery materials for improved electrochemical performance: A review. *Results Eng.* **2022**, *15*, 100472. [[CrossRef](#)]
3. Hu, Z.L.; Zhang, S.; Zhang, C.J.; Cui, G.L. High performance germanium-based anode materials. *Coordin. Chem. Rev.* **2016**, *326*, 34–85. [[CrossRef](#)]
4. Ye, J.; Chen, Z.; Hao, Q.; Xu, C.; Hou, J. One-step mild fabrication of porous core shelled Si-TiO₂ nanocomposite as high-performance anode for Li-ion batteries. *J. Colloid Interface Sci.* **2019**, *536*, 171–179. [[CrossRef](#)]
5. Hao, Q.; Hou, J.; Ye, J.; Yang, H.; Du, J.; Xu, C. Hierarchical macroporous Si/Sn composite: Easy preparation and optimized performances towards lithium storage. *Electrochim. Acta* **2019**, *306*, 427–436. [[CrossRef](#)]
6. Liu, D.; Liu, Z.; Li, X.; Xie, W.; Wang, Q.; Liu, Q.; Fu, Y.; He, D. Group IVA element (Si, Ge, Sn)-based alloying/dealloying anodes as negative electrodes for full-cell lithium-ion batteries. *Small* **2017**, *13*, 1702000. [[CrossRef](#)]

7. Wu, S.; Han, C.; Iocozzia, J.; Lu, M.; Ge, R.; Xu, R.; Lin, Z. Germanium-Based Nanomaterials for Rechargeable Batteries. *Angew. Chem. Int. Ed.* **2016**, *55*, 7898–7923. [[CrossRef](#)]
8. Chou, C.-Y.; Hwang, G.S. On the origin of the significant difference in lithiation behavior between silicon and germanium. *J. Power Sour.* **2014**, *263*, 252–258. [[CrossRef](#)]
9. Graetz, J.; Ahn, C.C.; Yazami, R.; Fultz, B. Nanocrystalline and thin film germanium electrodes with high lithium capacity and high rate capabilities. *J. Electrochem. Soc.* **2004**, *151*, A698–A702. [[CrossRef](#)]
10. Li, D.; Wang, H.; Zhou, T.; Zhang, W.; Liu, H.; Guo, Z. Unique structural design and strategies for germanium-based anode materials toward enhanced lithium storage. *Adv. Energy Mater.* **2017**, *7*, 1700488. [[CrossRef](#)]
11. Kennedy, T.; Mullane, E.; Geaney, H.; Osia, M.; O'Dwyer, C.; Ryan, K.M. High-performance germanium nanowire-based lithium-ion battery anodes extending over 1000 cycles through in situ formation of a continuous porous network. *Nano Lett.* **2014**, *14*, 716–723. [[CrossRef](#)] [[PubMed](#)]
12. O'Regan, C.; Biswas, S.; Petkov, N.; Holmes, J.D. Size-controlled growth of germanium nanowires from ternary eutectic alloy catalysts. *J. Mater. Chem. C* **2014**, *2*, 4597–4605. [[CrossRef](#)]
13. Collins, G.; Kolesnik, M.; Krstic, V.; Holmes, J.D. Germanium Nanowire Synthesis from Fluorothiolate-Capped Gold Nanoparticles in Supercritical Carbon Dioxide. *Chem. Mater.* **2010**, *22*, 5235. [[CrossRef](#)]
14. Wu, M.; Vanhoutte, G.; Brooks, N.R.; Binnemans, K.; Franssaer, J. Electrodeposition of germanium at elevated temperatures and pressures from ionic liquids. *Phys. Chem. Chem. Phys.* **2015**, *17*, 12080–12089. [[CrossRef](#)] [[PubMed](#)]
15. Vlaic, C.A.; Ivanov, S.; Peipmann, R.; Eisenhardt, A.; Himmerlich, M.; Krischok, S.; Bund, A. Electrochemical lithiation of thin silicon-based layers potentiostatically deposited from ionic liquid. *Electrochim. Acta* **2015**, *168*, 403–413. [[CrossRef](#)]
16. Al-Salman, R.; Mallet, J.; Molinari, M.; Fricoteaux, P.; Martineau, F.; Troyon, M.; Zein, S.; Abedin, E.; Endres, F. Template assisted electrodeposition of germanium and silicon nanowires in an ionic liquid. *Phys. Chem. Chem. Phys.* **2008**, *10*, 6233. [[CrossRef](#)]
17. Li, X.; Meng, G.; Xu, Q.; Kong, M.; Zhu, X.; Chu, Z.; Li, A.-P. Controlled Synthesis of Germanium Nanowires and Nanotubes with Variable Morphologies and Sizes. *Nano Lett.* **2011**, *11*, 1704–1709. [[CrossRef](#)]
18. Al-Salman, R.; Sommer, H.; Brezesinski, T.; Janek, J. Template-Free Electrochemical Synthesis of High Aspect Ratio Sn Nanowires in Ionic Liquids: A General Route to Large-Area Metal and Semimetal Nanowire Arrays. *Chem. Mater.* **2015**, *27*, 3830–3837. [[CrossRef](#)]
19. Liang, X.; Kim, Y.; Gebergziabihir, D.; Stickney, J. Aqueous Electrodeposition of Ge Monolayers. *Langmuir* **2010**, *26*, 2877–2884. [[CrossRef](#)]
20. Gavrillin, I.M.; Kudryashova, Y.O.; Kuz'mina, A.A.; Kulova, T.L.; Skundin, A.M.; Emets, V.V.; Volkov, R.L.; Dronov, A.A.; Borgardt, N.I.; Gavrillov, S.A. High-rate and low-temperature performance of germanium nanowires anode for lithium-ion batteries. *J. Electroanal. Chem.* **2021**, *888*, 115209. [[CrossRef](#)]
21. Gu, J.; Collins, S.M.; Carim, A.I.; Hao, X.; Bartlett, B.M.; Maldonado, S. Template-free preparation of crystalline Ge nanowire film electrodes via an electrochemical liquid-liquid-solid process in water at ambient pressure and temperature for energy storage. *Nano Lett.* **2012**, *2*, 4617–4623. [[CrossRef](#)] [[PubMed](#)]
22. Mahenderkar, N.K.; Liu, Y.-C.; Koza, J.A.; Switzer, J.A. Electrodeposited germanium nanowires. *ACS Nano* **2014**, *8*, 9524–9530. [[CrossRef](#)] [[PubMed](#)]
23. DeMuth, J.; Fahrenkrug, E.; Maldonado, S. Controlling nucleation and crystal growth of Ge in a liquid metal solvent. *Cryst. Growth Des.* **2016**, *16*, 7130–7138. [[CrossRef](#)]
24. Schmidt, V.; Gösele, U. How Nanowires Grow. *Science* **2007**, *316*, 698–699. [[CrossRef](#)] [[PubMed](#)]
25. Carim, A.I.; Collins, S.M.; Foley, J.M.; Maldonado, S. Benchtop electrochemical liquid-liquid-solid growth of nanostructured crystalline germanium. *J. Am. Chem. Soc.* **2011**, *133*, 13292–13295. [[CrossRef](#)]
26. Ma, L.; Gu, J.; Fahrenkrug, E.; Maldonado, S. Electrochemical liquid-liquid-solid deposition of crystalline Ge nanowires as a function of Ga nanodroplet size. *J. Electrochem. Soc.* **2014**, *161*, D3044–D3050. [[CrossRef](#)]
27. Acharya, S.; Ma, L.; Maldonado, S. Critical factors in the growth of hyperdoped germanium microwires by ec-LLS. *ACS Appl. Nano Mater.* **2018**, *1*, 5553–5561. [[CrossRef](#)]
28. DeMuth, J.; Ma, L.; Lancaster, M.; Acharya, S.; Cheek, Q.; Maldonado, S. Eutectic-bismuth indium as a growth solvent for the electrochemical liquid-liquid-solid deposition of germanium microwires and coiled nanowires. *Cryst. Growth Des.* **2018**, *18*, 677–685. [[CrossRef](#)]
29. Gromov, D.G.; Gavrillov, S.A. Heterogeneous Melting in Low-Dimensional Systems and Accompanying Surface Effects. In *Thermodynamics—Physical Chemistry of Aqueous Systems*, 1st ed.; Moreno Piraján, J.C., Ed.; INTECH Open Access Publisher: London, UK, 2011; Volume Chapter 7, pp. 157–190.
30. Gavrillin, I.M.; Gromov, D.G.; Dronov, A.A.; Dubkov, S.V.; Volkov, R.L.; Trifonov, A.Y.; Borgardt, N.I.; Gavrillov, S.A. Effect of electrolyte temperature on the cathodic deposition of Ge nanowires on In and Sn particles in aqueous solutions. *Semiconductors* **2017**, *51*, 1067–1071. [[CrossRef](#)]
31. Moulder, J.F. *Handbook of X-ray Photoelectron Spectroscopy: A Reference Book of Standard Spectra for Identification and Interpretation of XPS Data*; Physical Electronics Division; Perkin-Elmer Corporation: Winona, MN, USA, 1992; 261p.
32. Prabhakaran, K.; Ogino, T. Oxidation of Ge (100) and Ge (111) surfaces: An UPS and XPS study. *Surf. Sci.* **1995**, *325*, 263–271. [[CrossRef](#)]

33. Yang, L.C.; Gao, Q.S.; Li, L.; Tang, Y.; Wu, Y.P. Mesoporous germanium as anode material of high capacity and good cycling prepared by a mechanochemical reaction. *Electrochem. Comm.* **2010**, *12*, 418–421. [[CrossRef](#)]
34. Lee, S.W.; Ryu, I.; Nix, W.D.; Cui, Y. Fracture of crystalline germanium during electrochemical lithium insertion. *Extreme Mech. Lett.* **2015**, *2*, 15–19. [[CrossRef](#)]
35. Uysal, M.; Cetinkaya, T.; Alp, A.; Akbulut, H. Production of Sn/MWCNT nano-composite anodes by pulse electrodeposition for Li-ion batteries. *Appl. Surf. Sci.* **2014**, *290*, 6–12. [[CrossRef](#)]
36. Gao, S.; Wang, N.; Li, S.; Li, D.; Cui, Z.; Yue, G.; Zhao, Y.A. Multi-Wall Sn/SnO₂@Carbon Hollow Nanofiber Anode Material for High-Rate and Long-Life Lithium-Ion Batteries. *Angew. Chem. Int. Ed.* **2020**, *59*, 2465–2472. [[CrossRef](#)]
37. Kulova, T.L.; Gavrilin, I.M.; Kudryashova, Y.O.; Skundin, A.M.; Gavrilov, S.A. Cyclability enhancement and decreasing the irreversible capacity of anodes based on germanium nanowires for lithium-ion batteries. *Mendeleev Commun.* **2021**, *31*, 842–843. [[CrossRef](#)]
38. Yan, Y.; Liu, Y.; Zhang, Y.; Qin, C.; Yu, H.; Bakenov, Z.; Wang, Z. Sn modified nanoporous Ge for improved lithium storage performance. *J. Colloid Interface Sci.* **2021**, *602*, 563–572. [[CrossRef](#)]
39. Zakharov, A.N.; Gavrilin, I.M. Electrochemical formation of germanium nanostructures using low-melting-point metal particles. In Proceedings of The Sixth Asian School-Conference on Physics and Technology of Nanostructured Materials, Vladivostok, Russia, 22–29 April 2022.
40. Khabazian, S.; Sanjabi, S.; Del Campo, F.J.; Martín, E.F.; Tonti, D. Single-step electrochemical liquid-liquid-solid-assisted growth of Ge-Sn nanostructures as a long-life anode material with boosted areal capacity. *ACS Appl. Energy Mater.* **2022**, *5*, 5589–5602. [[CrossRef](#)]
41. Bahmani, E.; Zakeri, A.; Aghdam, A.S.R. Microstructural analysis and surface studies on Ag-Ge alloy coatings prepared by electrodeposition technique. *J. Mater. Sci.* **2021**, *56*, 6427–6447. [[CrossRef](#)]
42. Zhao, F.; Xu, Y.; Mibus, M.; Zangari, G. The Induced Electrochemical Codeposition of Cu-Ge Alloy Films. *J. Electrochem. Soc.* **2017**, *164*, D354–D361. [[CrossRef](#)]

Disclaimer/Publisher’s Note: The statements, opinions and data contained in all publications are solely those of the individual author(s) and contributor(s) and not of MDPI and/or the editor(s). MDPI and/or the editor(s) disclaim responsibility for any injury to people or property resulting from any ideas, methods, instructions or products referred to in the content.